

Experimental evidence of transient growth of energy before airfoil flutter

P. Hémon*, E. de Langre, P. Schmid

Département de Mécanique, LadHyX, Ecole Polytechnique – CNRS, 91128 Palaiseau, France

Received 29 September 2004; accepted 26 November 2005

Available online 24 January 2006

Abstract

This paper presents experimental evidence of the transient growth of energy for the coupled-mode flutter of an airfoil. The phenomenon occurs even in linearly stable dynamical systems. Its application is new in the context of fluid–structure interactions where only theoretical and numerical studies of transient growth exist. The experimental set-up allows an NACA 0015 airfoil to oscillate in rotational and vertical degrees of freedom when it is subjected to air-flow. Measurements consist of time series of the two motions obtained by laser displacement sensors. Structural parameters are first estimated without air-flow. The transient evolution of energy is measured, and amplification is observed for a given set of initial conditions. Our experiments agree well with numerical simulations based on unsteady airfoil theory.

© 2005 Elsevier Ltd. All rights reserved.

Keywords: Transient growth; Flutter instability

1. Introduction

In linear flutter studies, it is common to assume that the system amplitude behaves exponentially in time, decaying or growing depending on the wind velocity. The analysis then follows a normal modes approach where the long time behaviour is sought, particularly the critical value of the wind velocity, which determines the limit between stable and unstable behaviour.

In the field of hydrodynamic stability (Butler and Farrell, 1992), it has been found in recent years that energy growth can transiently occur in the subcritical parameter range of linear systems. This was mathematically formalized by Schmid and Henningson (2001) and references therein. This mechanism leads to an initial amplification of energy of the system, followed by monotonic decay due to the asymptotic stability of the system. This phenomenon is referred to as transient growth of energy.

Transient growth may be observed in dynamical systems that are generated by nonnormal operators. These systems have a set of nonorthogonal eigenfunctions, and any initial conditions expressed in this eigenfunction basis may undergo short-term amplification—despite the absence of unstable eigenvalues—which stems from an initial cancellation of multiple modes that ceases to exist as time progresses. This behaviour is inherent to the system and cannot be captured by considering individual modes and their corresponding eigenvalues. The asymptotic long-time

*Corresponding author. Tel.: +33 1 69 33 36 79; fax: +33 1 69 33 30 30.

E-mail address: pascal.hemon@ladhyx.polytechnique.fr (P. Hémon).

Nomenclature		U	wind velocity (m/s)
A_i	aeroelastic coefficients for pitching moment ($i = 1, \dots, 4$)	U_c	critical wind velocity (onset of flutter) (m/s)
b, c	span and chord of the profile (m)	z	vertical coordinate of centre of gravity (m)
C'_z	derivative of lift coefficient	<i>Greek symbols</i>	
d	distance between centre of gravity G and axis of rotation O (m)	α	angle of rotation (rad)
E	mechanical energy (J)	η	reduced structural damping
F_z	lift force (N)	λ	eigenvalue (rad^2/s^2)
f	frequency (Hz)	ρ	air density (kg/m^3)
H_i	aeroelastic coefficients for lift force ($i = 1, \dots, 4$)	ω	angular frequency (rad/s)
J_O	inertia of the rotational motion around O (kg m^2)	<i>Subscripts</i>	
k	stiffness (N m/rad) or (N/m)	0	initial conditions
M_O	pitching moment at axis of rotation O (N m)	1 or 2	coupled motions
m	mass involved in the vertical motion (kg)	z	pure vertical motion
		α	pure rotational motion

behaviour, though, is governed by the least stable eigenvalue. In physical terms, the linear system supports dynamics that cannot be described by purely exponential behaviour and that manifests itself in a composite, multi-modal response to initial conditions.

Theoretical and numerical studies were recently performed on various fluid–structure systems, which showed the possibility of transient growth in this kind of applications (Schmid and de Langre, 2003; Hémon and Noger, 2004). From an engineering point of view, transient growth might explain the premature structural fatigue encountered in structures subjected to wind. Another important feature of transient growth is that, if the growth is sufficiently large, a nonlinear instability can be triggered, even if the system is linearly stable at small amplitudes. This scenario could be interpreted as a by-pass mechanism leading to flutter instability below the linear critical velocity.

The objective of this paper is to present for the first time experimental evidence of transient growth for the coupled-mode flutter of an airfoil. Starting from this standard application, it is reasonable to believe that transient growth may be present for other kinds of elongated structures that are susceptible to coupled-mode flutter when subjected to cross-flow. Preliminary results of this study were presented at the 5th Colloquium on Bluff Body Aerodynamics and Applications, Ottawa, Canada, July 11–15, 2004.

The paper is organized as follows. First we describe airfoil flutter using a standard model. The experimental set-up and the results are then described and discussed in Section 3 and compared to numerical simulations of the problem.

2. Classical airfoil flutter

2.1. Structural modelling

We recall in this section the main features of coupled flutter of an airfoil, which can simultaneously oscillate transversely to the flow and in torsion, as shown Fig. 1. The axis of rotation and the centre of gravity are separated by a distance d , which induces structural coupling between the two degrees of freedom z and α . The equations of motion read [see Fung (1993)]:

$$\begin{aligned} m\ddot{z} + 2m\eta_z\omega_z\dot{z} + k_z z + md\ddot{\alpha} &= F_z, \\ J_O\ddot{\alpha} + 2J_O\eta_\alpha\omega_\alpha\dot{\alpha} + k_\alpha\alpha + md\ddot{z} &= M_O. \end{aligned} \quad (1)$$

The eigenvalues for the noncoupled case ($d = 0$) are

$$\lambda_\alpha = \omega_\alpha^2 = (2\pi f_\alpha)^2 = k_\alpha/J_O, \quad \lambda_z = \omega_z^2 = (2\pi f_z)^2 = k_z/m. \quad (2)$$

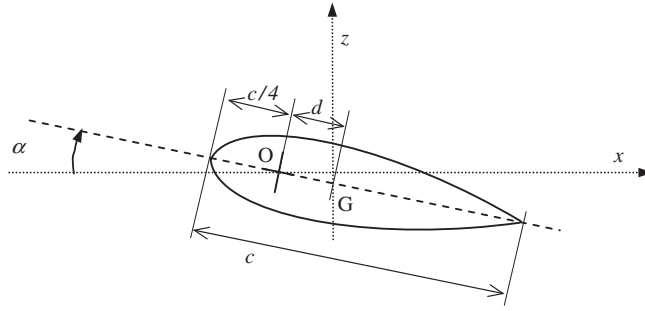


Fig. 1. Airfoil geometry.

For the more general coupled case, it can be shown that the distance d between the centre of gravity and the axis of rotation modifies the eigenvalues, so that

$$\lambda_1 + \lambda_2 = \lambda_z + \lambda_\alpha \frac{1}{1 - md^2/J_O}, \tag{3}$$

where the eigenvalues of the coupled system are λ_1 and λ_2 .

The total energy is the sum of kinetic and potential energy, which reads

$$E(t) = \frac{1}{2}m\dot{z}^2(t) + \frac{1}{2}J_O\dot{\alpha}^2(t) + md\dot{\alpha}(t)\dot{z}(t) + \frac{1}{2}k_z z^2(t) + \frac{1}{2}k_\alpha \alpha^2(t). \tag{4}$$

This quantity will be used to quantify transient growth. It will be nondimensionlized by the initial energy E_0 determined from the initial conditions. The maximum value of $E(t)$, as observed from the time series, will be denoted as E_{\max} .

2.2. Aerodynamic effect

The linear aerodynamic loads can be modelled using Scanlan’s (Scanlan and Tomko, 1971) flutter derivatives

$$\begin{aligned} F_z &= \frac{1}{2}\rho bcU^2(H_1\dot{z} + H_2\dot{\alpha} + H_3\alpha + H_4z), \\ M_O &= \frac{1}{2}\rho bc^2U^2(A_1\dot{z} + A_2\dot{\alpha} + A_3\alpha + A_4z), \end{aligned} \tag{5}$$

where the flutter derivatives, or aeroelastic coefficients, can be expressed with the help of Unsteady Airfoil Theory (UAT). The reduced velocity is defined based on the profile chord and the frequency of each pure motion, i.e.,

$$U_r = \frac{U}{cf_z} \quad \text{or} \quad U_r = \frac{U}{cf_\alpha}. \tag{6}$$

All the aeroelastic coefficients of Eq. (5) are expressed using the Theodorsen function (Theodorsen, 1935) $C(K) = F(K) + iG(K)$, where the reduced circular frequency is $K = 2\pi/U_r$. After some manipulations, this leads to (Fung, 1993)

$$\begin{aligned} H_1 &= \frac{-1}{U} C'_z F, & H_2 &= \frac{c}{U} C'_z \left[\frac{1}{4} + \frac{G}{K} + \frac{F}{2} \left(\frac{1}{2} - a \right) \right], \\ H_3 &= C'_z \left[F - \frac{KG}{2} \left(\frac{1}{2} - a \right) + K^2 \frac{a}{8} \right], & H_4 &= \frac{1}{c} C'_z \left[\frac{1}{4} + \frac{G}{K} \right] K^2, \\ A_1 &= \frac{-1}{U} C'_z \frac{F}{2} \left(\frac{1}{2} + a \right), & A_2 &= \frac{c}{U} C'_z \left[\frac{1}{8} \left(\frac{1}{2} - a \right) - \frac{G}{K} \frac{1}{2} \left(\frac{1}{2} + a \right) + \frac{F}{4} \left(a^2 - \frac{1}{4} \right) \right], \\ A_3 &= C'_z \left[\frac{1}{16} \left(a^2 + \frac{1}{8} \right) K^2 + \frac{F}{2} \left(\frac{1}{2} + a \right) + \frac{KG}{4} \left(a^2 - \frac{1}{4} \right) \right], & A_4 &= C'_z \frac{K^2}{2c} \left[\frac{a}{4} + \frac{G}{K} \left(\frac{1}{2} + a \right) \right]. \end{aligned} \tag{7}$$

The parameter a is the dimensionless distance between the axis of rotation O and the mid-chord location based on a reference length $c/2$. It is equal to $-1/2$ in our case. Note also that for an NACA 0015 profile, the aerodynamic centre is located at the forward quarter-chord point, which also coincides with the axis of rotation O .

In practice, the terms H_4 and A_4 have a negligible influence at large reduced velocities for our chosen range of parameters. Moreover, it can be useful to introduce the Quasi-Steady Theory assumption (Fung, 1993) in order to simplify the above expressions, hence

$$\begin{aligned} H_1 &= \frac{-1}{U} C'_z, & H_2 &= 0, & H_3 &= C'_z, & H_4 &= 0, \\ A_1 &= 0, & A_2 &= \frac{-1}{8} \frac{c}{U} C'_z, & A_3 &= 0, & A_4 &= 0. \end{aligned} \tag{8}$$

The static lift derivative C'_z is theoretically equal to 2π for a thin profile at low angle of attack within the assumptions of potential flow. But in practice, its value depends on the Reynolds number, especially in the lower parameter range of our experiments.

Combining Eqs. (1), (5) and (8), we have

$$\begin{aligned} \ddot{z} + 2\omega_z(\eta_z + \eta_{az})\dot{z} + \omega_z^2 z + d\ddot{\alpha} &= \frac{\rho b U_r^2}{2c f_z^2 m} C'_z \alpha, \\ \ddot{\alpha} + 2\omega_\alpha(\eta_\alpha + \eta_{\alpha z})\dot{\alpha} + \omega_\alpha^2 \alpha + \frac{md}{J_O} \ddot{z} &= 0, \end{aligned} \tag{9}$$

in which the uncoupled added aerodynamic dampings have been rewritten in the form of a reduced damping, such that

$$\eta_{az} = \frac{\rho b c^2}{2m} U_r, \quad \eta_{\alpha z} = \frac{\rho b c^4}{64 J_O} U_r. \tag{10}$$

2.3. Critical flutter velocity of the undamped system

In a first step, the critical velocity is deduced from the undamped coupled system (9), which is reduced to

$$\begin{aligned} \ddot{z} + \omega_z^2 z + d\ddot{\alpha} &= \frac{\rho b U_r^2}{2c f_z^2 m} C'_z \alpha, \\ \ddot{\alpha} + \omega_\alpha^2 \alpha + \frac{md}{J_O} \ddot{z} &= 0. \end{aligned} \tag{11}$$

Onset of flutter for this system arises when the eigenvalues become complex, at which time the two frequencies become equal. This occurs when

$$\det \begin{vmatrix} \lambda - \lambda_z & \lambda d + \frac{\rho b U_r^2}{2c f_z^2 m} H_3 \\ \frac{\lambda m d}{J_O} & \lambda - \lambda_\alpha \end{vmatrix} = 0, \tag{12}$$

which leads to finding the smallest root U^2 of the second-order equation

$$\left(\lambda_z + \lambda_\alpha + \frac{d\rho b c U^2}{2J_O} C'_z \right)^2 - 4\lambda_\alpha \lambda_z \left(1 - \frac{md^2}{J_O} \right) = 0. \tag{13}$$

The critical velocity is finally given by

$$U_c^2 = \frac{-2J_O \left(-(\lambda_z + \lambda_\alpha) + \sqrt{4\lambda_\alpha \lambda_z \frac{\lambda_z + \lambda_\alpha}{\lambda_1 + \lambda_2}} \right)}{\rho b c d C'_z}, \tag{14}$$

and the frequency of flutter, determined for the critical velocity, is

$$f_c^2 = \frac{1}{(2\pi)^2} \sqrt{\lambda_\alpha \lambda_z \frac{\lambda_1 + \lambda_2}{\lambda_z + \lambda_\alpha}}. \tag{15}$$

3. Experimental evidence

3.1. Experimental set-up

The wing profile is a NACA 0015 with a chord of 0.12 m and a 0.17 m span. It is built from Plexiglas using a numerical milling machine. The resulting surface is smooth without artificial roughness. The profile is mounted in a small Eiffel wind tunnel with a closed square test-section of 0.180 m width. The wind stream is produced by a centrifugal fan with an electric power of 2500 W mounted downstream and exhausting the air-flow vertically. The mean velocity in the test-section can vary from 2 to 25 m/s, with a turbulence level of 1.5% at 10 m/s.

The axis of rotation of the profile is located at its forward quarter-chord and passed through the wind tunnel walls inside two vertical fences. The axis is suspended via bearings at the extremities of two long flat bands of aluminium alloy, such as laminated springs (see Fig. 2). Their length, width and thickness is 400, 20 and 2 mm, respectively. Adjustment of the frequency was accomplished by adjusting the thickness to approximately 1 mm near the clamping using a milling machine. The torsion frequency is set by two series of linear springs.

The measurements are obtained from two laser displacement sensors, one for the vertical bending motion, and the other one for the combined movement of torsion and bending. The measurement resolution is 40 μm and the accuracy is better than 1% of the full-scale range (± 10 mm). The output signals of these sensors are digitized with a PAK system provided by Müller BBM (24 bits resolution). The sampling frequency was chosen as 512 Hz, and a DC coupling is used in both channels. Recovery of the physical quantities in terms of vertical position, angle of torsion and energy is performed directly within the measurement system by numerical post-processing.

Transient records are triggered automatically so that the starting point is repeatable, and initial conditions are recorded through the DC coupling of the measurement chain. Note that in the computation of the energy, it is essential to ensure that the system at rest (without wind) provides a zero constant signal, due to the necessary differentiation process for obtaining the velocities.

3.2. Identification of structural parameters

The structural parameters are determined without wind. First we deal with the two motions separately. We measure the natural frequencies f_z and f_α by spectral analysis and the stiffness k_z and k_α by static calibration. Then, we deduce the inertia J_O and m from Eq. (2).

The frequencies f_1 and f_2 of the coupled system are then measured and the distance d is deduced from Eq. (3). The results are given in Table 1.

Structural damping is measured for each degree of freedom independently. For vertical motion, the system has a very low damping of $\eta_z = 0.40\%$. For torsion, the mechanical assembly, especially the bearings, introduce damping, which is found to be a function of the amplitude of the oscillations. It varies from 10% for amplitudes around 2° to 6% for higher amplitudes around 7° .

In order to validate these results, we reproduce an experimental test without wind by numerical simulation and compare the results in Fig. 3. The initial condition is a small vertical offset in the downward direction, leading to a nonzero initial value for z and a small positive angle of torsion, as a consequence of the coupled mechanical system. It

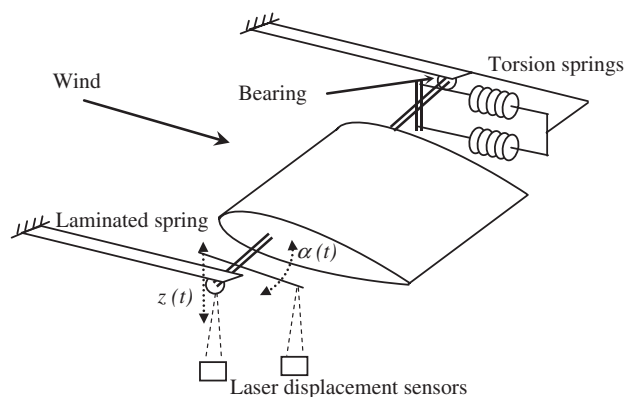


Fig. 2. Experimental set-up.

Table 1
Measured structural parameters

f_z (Hz)	f_z (Hz)	k_x (N m/rad)	k_z (N/m)	f_1 (Hz)	f_2 (Hz)	J_O (kg m ²)	m (kg)	d (m)
2.597	3.613	0.1140	436.0	2.441	4.004	0.00042365	0.846	-0.00706

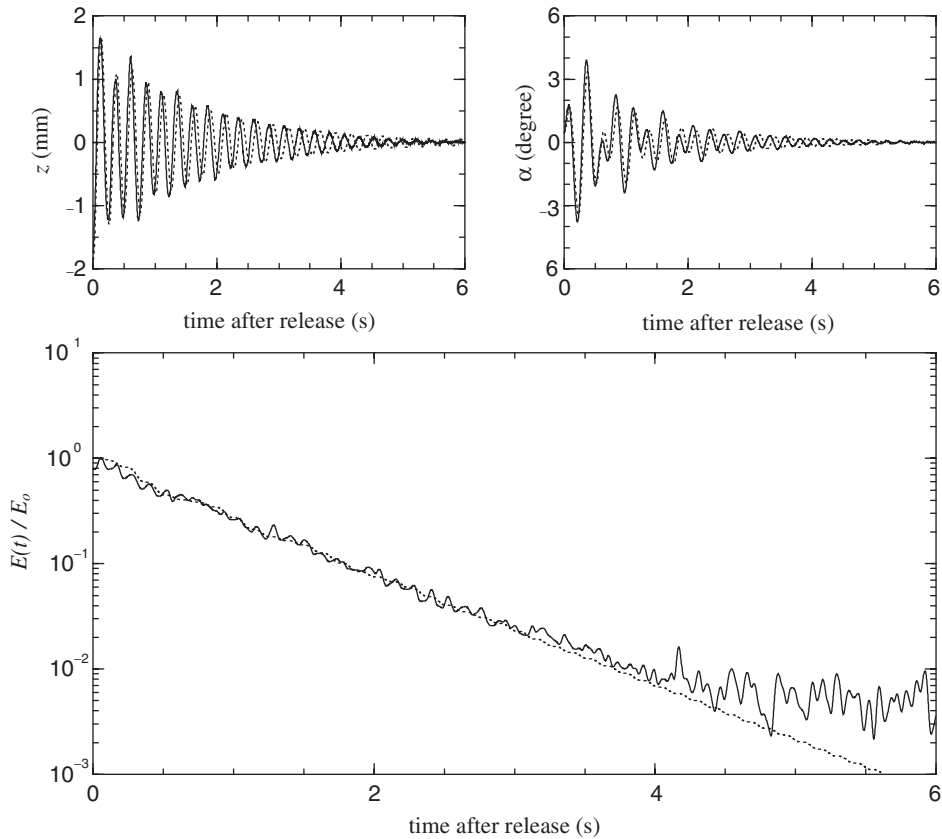


Fig. 3. Time history of vertical displacement, angle of rotation and corresponding dimensionless total energy without wind ($U = 0$). Initial conditions are $z_0 = -1.85$ mm, $\alpha_0 = 0.5^\circ$. —, Experiments; , computation using Eq. (1).

should be mentioned that, because of the laminated spring, a vertical displacement induces a small angle of rotation, which is taken into account in the recovery procedure of the pitch angle α .

In the experiments, the initial energy is weakly perturbed by the DC value of the measured components, leading to spurious oscillations during the decay. It will be seen later that these perturbations can be treated as noise and that the signal of interest is substantially larger. In Fig. 3, the agreement between experimental and numerical results is very good and thus validates the measured structural parameter values. It is of importance to note that the relevant energy in this approach is the total energy as defined by Eq. (4), not any of its components which all oscillate in time.

3.3. Identification of aerodynamic damping and critical velocity

The experimental critical velocity U_c is found to be 9.0 m/s, compared to 7.83 m/s given by Eq. (14) using the lift slope $C'_z = 2\pi$. Two reasons may cause the difference: (i) the effect of damping, especially in torsion, which has a stabilizing effect and increases the critical velocity; (ii) a Reynolds number effect ($Re = 72\,000$ at the onset of flutter) because the

laminar–turbulent transition of the boundary layer over the profile has a significant influence on the lift slope in this regime.

However, the numerical simulations of the full model (7) lead to a critical velocity equal to 9.28 m/s in very good agreement with the experiments. Therefore, the numerical simulations shown later in this paper will be based on Eq. (7), taking into account all relevant terms.

Good agreement is obtained for the flutter frequency: 3.26 Hz (experimental), versus 3.145 Hz (Eq. (15)). Note that this frequency was experimentally determined at a velocity just before the onset of flutter, in order to make the measurements with a nondiverging system.

For the added damping, agreement with relations (10) and experiments is also good. For vertical motion, the experimental value is 1.98% at $U_r = 21$, compared to 1.82% from theoretical calculations. For torsion, the added damping at $U_r = 29$ is approximately 3.5% compared to the theoretical value of 4.52%, but a high experimental uncertainty due to the high structural damping at zero velocity should be expected.

3.4. Transient growth measurements

We proceed by applying the initial conditions in z and α , as described above, to the system with several wind velocities just under the critical velocity. A typical time series is shown in Fig. 4, where an amplification of the energy by a factor of about 2 can clearly be observed. At the same time, the angle of attack reaches a value of nearly 6° , whereas it remained under 4° without wind, see Fig. 3. This is consistent with the fact that an amplification of energy by a factor of 2 induces an amplification by a factor of $\sqrt{2}$ of the displacement.

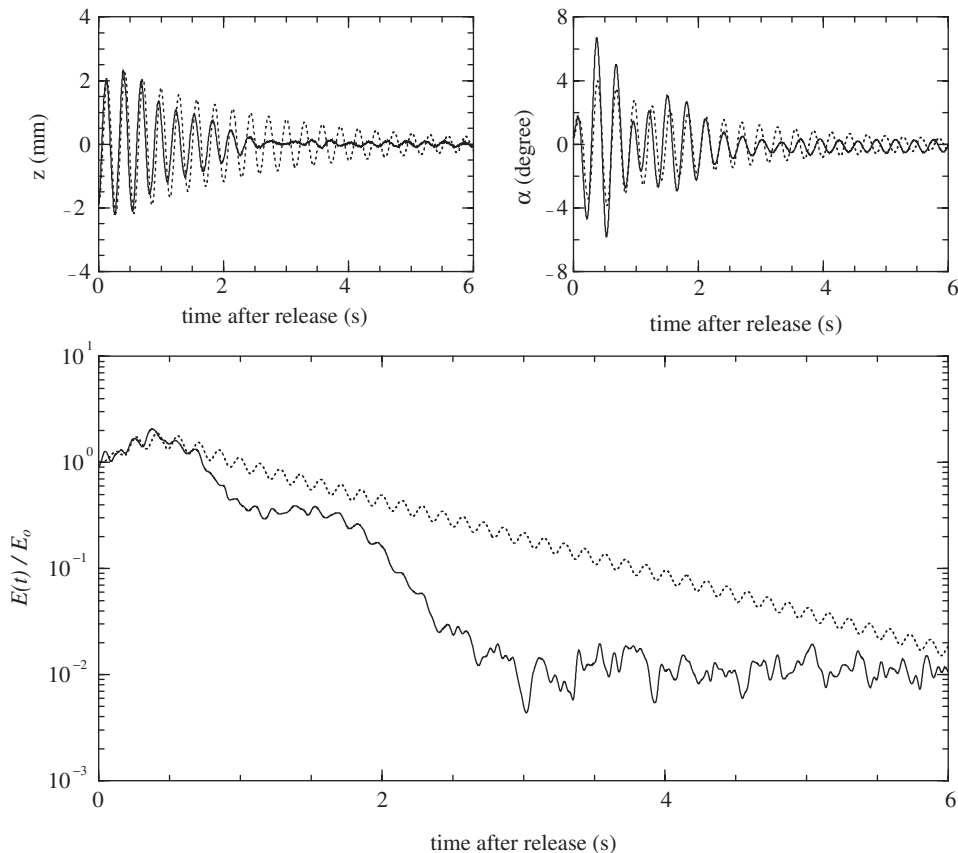


Fig. 4. Time history of vertical displacement, angle of rotation and corresponding dimensionless total energy with $U/U_c = 0.92$. Initial conditions as in Fig. 3. —, Experiments; , computation using UAT, Eqs. (1), (5) and (7).

In Fig. 5, the maximum amplification of energy is plotted for a number of tests versus the velocity parameter $1 - U/U_c$ as defined by Schmid and de Langre (2003). In the experiments, the amplification occurs for velocity parameters below 0.30 and the amplification reaches a saturation value of about 2.5 just before the onset of flutter.

The numerical simulation using UAT, Eq. (7), demonstrates a remarkable agreement with experiments. This shows that for transient behaviour simulations, it is essential to account for all coefficients H_i and A_i , including those that are usually considered negligible in the long-term stability problem.

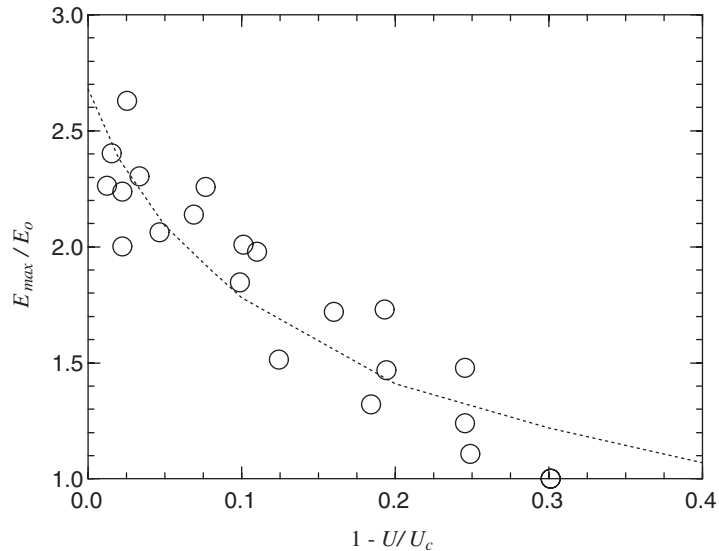


Fig. 5. Maximum amplification of energy E_{max}/E_0 versus velocity parameter $1 - U/U_c$ for initial conditions $z_0 = -1.85$ mm and $\alpha_0 = 0.5^\circ$. \circ , Experiments; computations using UAT.

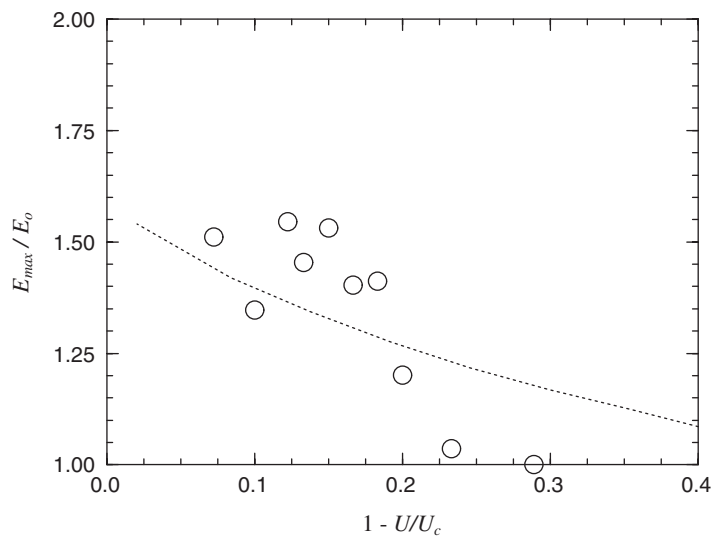


Fig. 6. Maximum amplification of energy E_{max}/E_0 versus velocity parameter $1 - U/U_c$ for initial conditions $z_0 = 0.5$ mm, $\alpha_0 = -1.6^\circ$, $\dot{z}_0 = -38$ mm/s and $\dot{\alpha}_0 = -60^\circ$ /s. \circ , Experiments; computations using UAT.

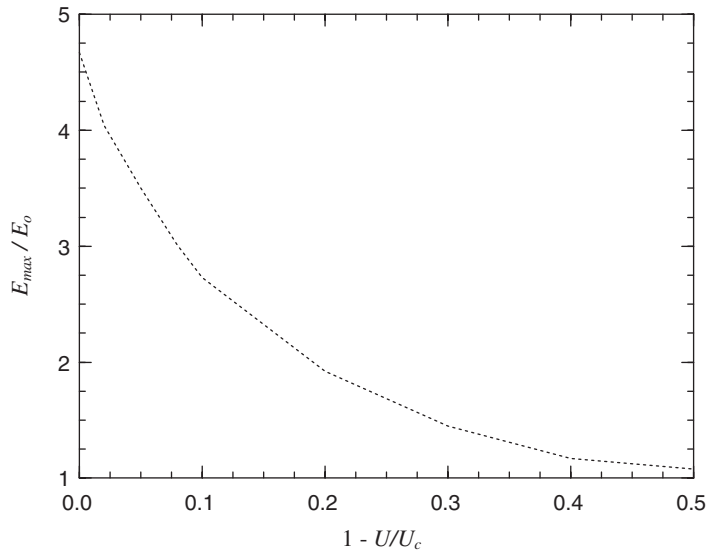


Fig. 7. Maximum amplification of energy E_{max}/E_0 versus velocity parameter $1 - U/U_c$. Computations using UAT for optimal initial conditions $z_0 = -2$ mm and $\alpha_0 = +6^\circ$.

3.5. Effect of the initial conditions

We now use a different set of initial conditions. The experimental procedure consists of dropping a small mass (50 g) on the profile from a given height. The measurement trigger remains linked to one of the channels. The purpose is to introduce initial conditions in velocities \dot{x} and \dot{z} with maximum repeatability.

This technique leads to the set of initial conditions $z_0 = 0.5$ mm, $\alpha_0 = -1.6^\circ$, $\dot{z}_0 = -38$ mm/s and $\dot{\alpha}_0 = -60^\circ$ /s. The maximum amplification of energy versus the velocity parameter is plotted in Fig. 6. Transient amplification of energy is clearly observed for the chosen parameter range and is in good agreement with theoretical predictions. Note that for this type of initial condition, the critical velocity cannot be approached, in practice, as much as in the preceding case. Still, theory predicts transient growth up to the critical velocity.

It is interesting to numerically determine the set of initial conditions that would lead to the maximum amplification rate. Exploring the space of all possible initial conditions, these were found to be $z_0 = -2$ mm, $\alpha_0 = 6^\circ$, $\dot{z}_0 = 0$ mm/s and $\dot{\alpha}_0 = 0^\circ$ /s. The corresponding amplification is shown in Fig. 7. We observe a saturation value of 4.6, which constitutes a rather large amplification.

It has been shown that transient growth can induce higher stresses in the structure than is usually admissible for a stable aeroelastic system. From an engineering point of view, a study of transient energy growth should be part of any design process of a structure, especially as far as the fatigue effects are concerned. It is also possible that a by-pass transition to an unstable regime can occur for systems with a subcritical unstable nonlinear branch.

4. Conclusion

We presented experimental evidence of transient growth of energy before coupled-mode flutter of an airfoil. This mechanism has been shown before for various fluid–structure systems using theoretical and numerical simulation, but without experimental proof. An experimental set-up was presented which allowed a NACA 0015 profile to oscillate in vertical motion and in torsion. The transient behaviour of this system starting with specified initial conditions showed a transient amplification of energy before the usual exponential decay. UAT was found to reliably capture the phenomenon, as long as all relevant terms are included in the simulations.

In terms of applications to vehicle aeroelasticity or wing flutter, the results presented here suggest that, even below the critical velocity, large amplitude vibrations may result from natural transient loading.

This phenomenon might explain some premature fatigue of wind-excited structures. Moreover, it could be responsible for a by-pass transition to an unstable regime by nonlinear amplitude effects. A study of transient growth is recommended for the fatigue analysis of structures that are submitted to wind loads.

References

- Butler, K.M., Farrell, B.F., 1992. Three-dimensional optimal perturbation in viscous shear flow. *Physics of Fluids A* 4, 1637–1650.
- Fung, Y.C., 1993. *An Introduction to the Theory of Aeroelasticity*. Dover, New York.
- Hémon, P., Noger, C., 2004. Transient growth of energy and aeroelastic stability of ground vehicles. *Comptes Rendus Mécanique* 332, 175–180.
- Scanlan, R.H., Tomko, J.J., 1971. Airfoil and bridge deck flutter derivatives. *ASCE Journal of the Engineering Mechanics Division* EM6, 1717–1737.
- Schmid, P.J., de Langre, E., 2003. Transient growth before coupled-mode flutter. *ASME Journal of Applied Mechanics* 70, 894–901.
- Schmid, P.J., Henningson, D.S., 2001. *Stability and Transition in Shear Flows*. Springer, New York.
- Theodorsen, T., 1935. General theory of aerodynamic instability and the mechanism of flutter. *NACA Technical Report* 496.